Synthesis and Characterization of TiO_2@C Core−Shell Composite Nanoparticles and Evaluation of Their Photocatalytic Activities

Sangaraju Shanmugam,[†] Alexandra Gabashvili,[†] David S. Jacob,[†] Jimmy C. Yu,[‡] and Aharon Gedanken*,[†]

Department of Chemistry and Kanbar Laboratory for Nanomaterials at the Bar-Ilan University Center for Advanced Materials and Nanotechnology, Bar-Ilan University, Ramat-Gan 52900, Israel, and Department of Chemistry, The Chinese University of Hong Kong, Shatin, NT, Hong, Kong, SAR, China

Received December 18, 2005. Revised Manuscript Received March 15, 2006

TiO_2@C core−shell composite nanoparticles were synthesized by a simple and efficient single-step method in a specially made Swagelok cell at different temperatures. The prepared samples were characterized by XRD, diffuse reflectance-UV−vis, Raman, TEM, HRTEM, and N_2 adsorption−desorption methods. The carbon content in the samples can be varied with reaction time and temperature. It is evident from TEM analysis that the as-prepared samples are core−shell structures of TiO_2, anatase phase, and C. The diameter of the TiO_2@C nanoparticles is in the range of 15−35 nm. HRTEM results showed that a few graphitic layers were wrapped on the surface of TiO_2, and these carbon layers are responsible for suppressing other phase formations of TiO_2 even at high temperature. However, a few percentage points of the rutile phase are observed at high temperature (900 °C), evidenced from Raman analysis. The prepared samples were tested for their photochemical activities for 4-chlorophenol degradation. The sample prepared at 700 °C showed comparable activity for the degradation of 4-chlorophenol with that of Degussa P25. The photobleaching studies of methylene blue were also carried out under sunlight. It was found that the TiO_2@C samples showed higher photocatalytic activity than Degussa P25.

1. Introduction

Nanostructured materials have received much attention in recent years due to their unusual properties such as optical, chemical, photoelectrochemical, and electronic properties.[1] Recently, TiO_2 was found to be a promising photocatalytic candidate for the photoelectrochemical splitting of water.[2] Nanosized anatase TiO_2 is most attractive for these applications because of its large effective surface area which enhances the catalytic activities.[3] It is reported that nanosized TiO_2 particles are also advantageous for more effective photogenerated carriers separation and greater photocurrent, yielding higher photocatalytic and photoelectrical efficiencies.[4] TiO_2 exists in three crystalline forms: anatase, rutile, and brookite. Among them anatase is the low-temperature phase, exhibiting properties which render it interesting for various applications such as photovoltaic cells[5] and photocatalysis[6] and for its antimicrobial properties.[7] Numerous studies have shown that anatase TiO_2 exhibits more superior photocatalytic activity than rutile.[8] The crystalline nature of anatase TiO_2 is important for various applications, and so high-temperature treatment is necessary to have better crystalline TiO_2 for catalytic reactions, especially in photocatalysis.

Several methods have been employed for improving the photocatalytic activity of TiO_2 such as increasing the surface area of TiO_2, generating defect sites, surface modification with metals, and addition of semiconducting metal oxides.[9] Supporting TiO_2 on various porous materials such as SiO_2, ZrO_2, zeolites, and activated carbons were used to increase the adsorption capacity of organic compounds.[10] It was reported by Inakagi et al.[11] that modification of TiO_2 surface by carbon coating has advantages such as stabilization of the anatase phase, high adsorptivity, and high photocatalytic activity. They prepared carbon-coated TiO_2 by heat treatment of a mixture of TiO_2 and various polymers (poly(vinyl

* To whom correspondence should be addressed. E-mail: gedanken@mail.biu.ac.il.
† Bar-Ilan University.
‡ The Chinese University of Hong Kong.

(1) Henglein, A. *Chem. Rev.* **1989**, *89*, 1861.; Weller, A. *Angew. Chem., Int. Ed. Eng.* **1993**, *32*, 41.
(2) O'Regan, B.; Gratzel, M. *Nature* **1991**, *353*, 737.
(3) Zhang, Z.; Wang, C. C.; Zakaria, R.; Ying, J. Y. *J. Phys. Chem. B* **1998**, *102*, 10871.
(4) Hoffmann, M. R.; Martin, S. T.; Choi, W.; Bahnemann, D. W. *Chem. Rev.* **1995**, *95*, 69. Linsebigler, L.; Lu, G.; Yates, J. T. *Chem. Rev.* **1995**, *95*, 735. Zhao, G.; Kozuka, H.; Yoko, T. *Thin Solid Films* **1996**, *277*, 147. Kaneko, M.; Okura, I. *Photocatalysis, Science and Technology*; Springer, Berlin, 2002. Serpone, N.; Pelizzetti, E. *Photocatalysis: Fundamentals and Applications*; Wiley: New York, 1989.
(5) Fujishima, A.; Rao, T. N.; Tryk, D. A. *J. Photochem. Photobiol. C* **2000**, *1*, 1.
(6) Gratzel, M. *Nature* **2001**, *414*, 338.
(7) Fu, G.; Vary, P. S.; Lin, C.-T. *J. Phys. Chem. B* **2005**, *109*, 8889.
(8) Zhu, J.; Zheng, W.; He, B.; Zhang, J.; Anpo, M. *J. Mol. Catal. A* **2004**, *216*, 35. Zhang, J.; Ayusawa, T.; Minagawa, M.; Kinugawa, K.; Yamashita, H.; Matsuoka, M.; Anpo, M. *J. Catal.* **2001**, *198*, 1. Zhang, J.; Hu, Y.; Matsuoka, M.; Yamashita, H.; Minagawa, M.; Hidaka, H.; Anpo, M. *J. Phys. Chem. B* **2001**, *105*, 8395. Park, D. R.; Zhang, J.; Ikeue, K.; Yamashita, H.; Anpo, M. *J. Catal.* **1999**, *185*, 114.
(9) Yu, J. C.; Zhang, L. Z.; Yu, J. G. *New. J. Chem.* **2002**, *26*, 416. Rusu, C. N.; Yates, J. T. *Langmuir* **1997**, *13*, 4311. Yu, J. C.; Lin, J.; Kowk, R. W. M. *J. Photochem. Photobiol. A: Chem.* **1997**, *111*, 199.
(10) Kasuga, T.; Hiramatsu, M.; Hirano, M, Hoson, A. *J. Mater. Res.* **1997**, *12*, 607. Toba, M.; Niwa, F.; Mizukami, S.; Sano, T.; Maeda, K.; Annila, A.; Kampa, V. *J. Mol. Catal.* **1994**, *91*, *277*,
(11) Inakagi, M.; Kojin, F.; Tryba, B.; Toyoda, M. *Carbon* **2005**, *43*, 1652.

10.1021/cm052790n CCC: $33.50
Published on Web 04/08/2006

alcohol), hydroxyl propyl cellose, and poly(ethylene terephthalate) at high temperatures under an inert atmosphere.[11] Visible-light-assisted photocatalytic activity was demonstrated by doping N, S, and C into substitutional sites in the crystal structure of anatase TiO_2.[12] Mechanical mixtures of anatase TiO_2 and carbon were shown to give a better performance for the decomposition of different model organic components.[13] Various studies have demonstrated that the TiO_2 mounted on C and coated on carbon showed different photocatalytic activities.[14] The inherent advantage of a few carbon layers wrapped on the TiO_2 is that the contaminant molecules have to be adsorbed first into the carbon layer, which covers the TiO_2 particle, and diffuse through the carbon to reach the active surface where it undergoes the actual reaction. When this approach was adopted, a coupling between photoactivity and adsorptivity was achieved in a single process. In the current paper we present a simple method for the preparation of TiO_2@C core−shell type composite materials by using a single-component precursor in a single-step process. The prepared composites were characterized with XRD, diffuse reflectance-UV−vis, Raman, TEM, HRTEM, and N_2 adsoption−desorption techniques. We have also studied the effect of temperature on the crystalline nature of TiO_2. The graphitic layers present on the surface of TiO_2 are responsible for phase suppression, even at high temperatures. The TiO_2@C composite materials were tested for the photocatalytic decomposition of 4-chlorophenol and methylene blue under visible irradiation and were compared with a commercial P25 sample.

2. Experimental Section

Preparation of TiO_2@C Core−Shell Nanoparticles. The syntheses of TiO_2@C core−shell composite (TC) samples were carried out in a specially made cell made of a Swagelok union. Titanium(IV) oxyacetyl acetonate monohydrate (Aldrich) was used as-received. The synthesis of TiO_2@C was carried out by introducing Ti(IV) oxyacetyl acetonate into a 2 mL closed vessel cell. The cell was assembled from stainless steel Swagelok parts. A $^3/_4$ in. union part was plugged from both sides by standard caps. For a typical synthesis, 0.5 g of starting material was introduced into the cell at atmospheric conditions. The filled cell was closed tightly with the other plug and then placed inside an iron pipe at the center of the furnace. The temperature was raised at a heating rate of 20 °C/min. The closed vessel cell was heated at different temperatures (700, 800, and 900 °C) for 3 h. The reaction took place at the autogenic pressure of the precursor. The closed vessel cell (Swagelok) heated at 700 °C was gradually cooled to room temperature and opened with the release of a little pressure, and 0.313 g of black powder was obtained. The total yield of the obtained material was 62% (relative to the starting material). Similar experiments were carried out at different temperatures such as 800 and 900 °C. The products obtained at temperatures of 700, 800, and 900 °C were named as TC-700, TC-800, and TC-900, respectively.

Structural Characterization. The X-ray diffraction measurements were carried out with a Bruker AXS D* Advance Powder X-ray diffractometer with a Cu Kα ($\lambda = 1.5418$ Å) radiation source. Diffraction patterns were collected from 20° to 80° at a speed of 1.2°/min. The average crystalline sizes of TC samples were calculated by using the Scherrer formula by taking the full-width at half-maximum (fwhm) of the anatase (101) diffraction peak. The diffuse reflectance-UV−vis (DRUV) spectra of samples were recorded on a Perkin-Elmer UV−visible spectrophotometer. Scanning electron microscopy (SEM) of the obtained products was carried out on a JEOL-JSM 840 scanning electron microscope operating at 10 kV. The particle morphology was studied with transmission electron microscopy on a JEOL-JEM 100 SX microscope, working at an 80 kV accelerating voltage, and a JEOL-2010 HRTEM, using an accelerating voltage of 200 kV. Samples for TEM and HRTEM measurements were prepared by ultrasonically dispersing the products into absolute ethanol, then placing a drop of this suspension onto a copper grid coated with an amorphous carbon film, and then drying in air. The elemental analysis of the sample was carried out by an Eager C, H, N, S analyzer. The Olympus BX41 (Jobin Yvon Horiba) Raman spectrometer was employed, using the 514.5 nm line of an Ar laser as the excitation source to analyze the nature of the carbon present in the products. The Brunauer−Emmett−Teller (BET) surface area measurements were performed by a Micromeritics (Gemini 2375) surface area analyzer. The nitrogen adsorption and desorption isotherms were measured at 77 K after degassing the samples by heating at 140 °C for 5 h.

Photocatalytic Experiments. The photocatalytic activity of the TC samples was tested for the degradation of 4-chlorophenol in aqueous solution. O_2 was bubbled into the solution throughout the experiment. A 300 W tungsten halogen lamp with a 400 nm cutoff filter was used as the light source. Then 0.2 g of a photocatalyst was suspended in a 200 mL aqueous solution of 2.2×10^{-4} M 4-chlorophenol. The concentrations of 4-chlorophenol and its degradation products were measured with an HPLC system (Waters Baseline 810) with a Waters 486 tunable UV absorbance detector. A Supelco LC-18-DB column (250 mm × 4.6 mm) was applied. The eluent consisted of a 40:60 methanol:water mixture and the flow rate was 1 mL/min. The aromatic compounds were detected at 220 nm. Millipore disks were used to separate the catalysts before analysis of the solution.

In addition, the photocatalytic activities of the samples were also evaluated by the degradation of methylene blue in an aqueous solution under sunlight. Fifty milligrams of TC samples was dispersed in 50 mL of methylene blue solution (2.5×10^{-5} mol/L) were stirred in the dark and fresh methylene blue solution was used for photobleaching studies. The mixture was stirred in visible light for stipulated time periods. The degradation of MB was monitored by a UV−visible spectrophotometer. Both reactions were also carried out on Degussa P25, which naturally consists of about 80% anatase and 20% rutile with a BET surface area of 55 m^2/g.

3. Results and Discussion

The carbon content in the TiO_2@C product obtained at 700 °C was 36.5 wt % as determined by C, H, and N elemental analysis. The calculated carbon content in the

(12) Asahi, R.; Morikawa, T.; Ohwaki, T.; Aoki, K.; Taga, Y. *Science* **2001**, *293*, 269. Rhee, C. H.; Bae, W. B.; Lee, J. S. *Chem. Lett.* **2005**, *34*, 660. Irie, H.; Watanabe, Y.; Hashimoto, K. *J. Phys. Chem. B* **2003**, *107*, 5483. Umebayashi, T.; Yamaki, T.; Tanaka, S. Asai, K. *Chem. Lett*. **2003**, *32*, 330. Ohno, T.; Misui, T.; Matsumura, M. *Chem. Lett*. **2003**, *32*, 364. Choi, Y.; Umebayashi, T.; Yoshikawa, M. *J. Mater. Sci.* **2004**, *39*, 1837.

(13) Herrmann, J. M.; Matos, J.; Disdier, J.; Guillard, C.; Laine, J.; Malato, S.; Blanco, J. *Catal. Today* **1999**, *54*, 255. Matos, J.; Laine, J.; Herrmann, J. M.; *J. Catal*. **2001**, *200*, 10.

(14) Takeda, N.; Torimoto, T.; Sampath, S.; Kubabara, S.; Yoneyama, H. *J. Phys. Chem*. **1995**, *99*, 9986. Torimoto, T.; Okawa, Y.; Takeda, N.; Yoneyama, H. *J. Photochem. Photobiol. A: Chem.* **1997**, *103*, 153. Harada, M.; Tanii, A.; Yamashita, H.; Anpo, M. *Z. Phys. Chem.* **1999**, *213*, 59.

Table 1. Physicochemical Characterization of TiO_2@C Samples

sample	phase XRD	C (%)	S_{BET} (m^2/g)	pore size[a] (nm)	pore volume[b] (cm^{-3}/g)	low-frequency Raman width (cm^{-1})	particle size (nm) TEM (±3)	particle size (nm) XRD (±2)	rate constant k (min^{-1})
TC-700	A	36.7	29	15	0.10	13.0	25	19.8	0.004
TC-800	A	34.7	26	29	0.12	14.0	20	19.5	0.010
TC-900	A	32.8	25	39	0.14	16.8	16	17.6	0.149

[a] BJH desorption average pore diameter. [b] Single-point total pore volume of the pores at P/P_0, 0.95.

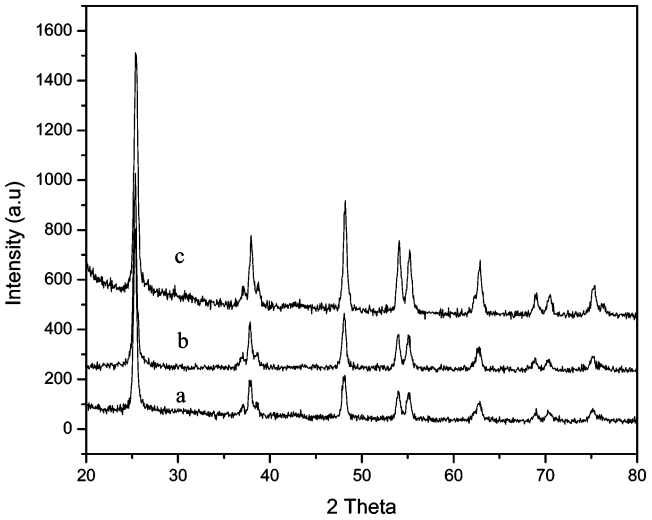

Figure 1. XRD patterns of TiO_2@C composites prepared at (a) 700, (b) 800, and (c) 900 °C.

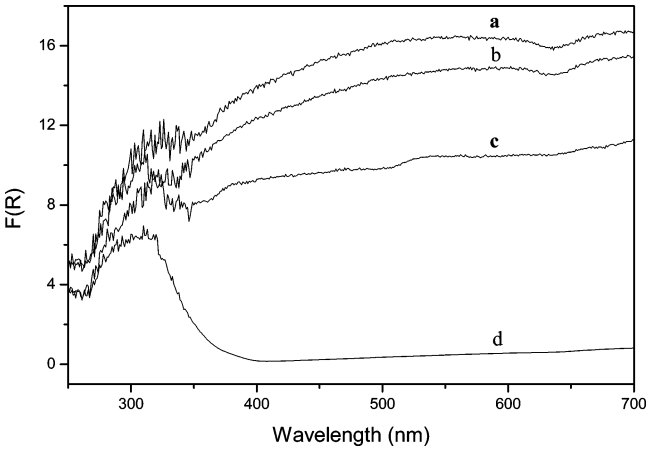

Figure 2. Diffusive reflectance-UV−vis spectra of TiO_2@C composites prepared at (a) 700, (b) 800, and (c) 900 °C and (d) commerical P25.

precursor was 45 wt %. A comparison of the carbon content in the products obtained at the various heating temperatures appears in Table 1. Figure 1 shows the XRD pattern of TC products prepared at different temperatures. Figure 1 illustrates that the TC-700, TC-800, and TC-900 products are composed of pure anatase TiO_2. The diffraction peaks were observed at $2\theta = 25.3$, 37.9, 48.15, 54.05, and 55.28° and are assigned as (101), (004), (200), (105), and (211) reflection planes of the body-centered tetragonal phase of TiO_2. It is seen from Figure 1 that the intensity of all peaks increased as the temperature increased, indicating the enhancement of the crystallinity of anatase titania. It is known that the phase transformation of anatase to rutile occurs at around 600 °C.[15] However, in the present study we observed that the anatase phase is sustained even above this transformation temperature. According to our interpretation, this is because of the carbon present on TiO_2 which suppresses the phase transformation, even at high temperature. It is interesting to note that anatase is the only phase observed from XRD measurements even when the reaction is conducted at 1000 °C (not shown). The suppression of phase transfer may be due to the presence of carbon shell around the TiO_2 nanoparticles. Similar results were reported by Inagaki et al.[16] They found that the minimal amount of coated carbon for the suppression of phase transformation is about 5 wt %. Anatase TiO_2 phase is kinetically stable and thermodynamically unstable and rutile is thermodynamically stable at high temperature. The carbon layers are acting as barriers for the phase transformation from anatase to rutile. It can be speculated that the energy that surmounts at high temperature is directly exposed to the carbon layers not to the TiO_2 core; thus, the core retains the anatase phase.

The average particle size was calculated by using the Scherrer equation[17] and taking the full-width at half-maximum diffraction peak of (101), and the obtained results are given in Table 1. It is well-known that only the anatase phase in TiO_2 shows high photocatalytic activity. Thus, the composites with a high level of anatase may have good photocatalytic activity.

Figure 2 shows the optical absorption of TC anatase samples compared with the absorption spectrum of P25. The spectra were measured in the reflection mode. P25 reveals an absorption edge around 350 nm as expected for anatase TiO_2. All TC samples absorb in the whole visible region due to the presence of carbon on TiO_2. The absorption edge of anatase TiO_2 can also be detected. The anatase peak is also shifted to higher wavelength for all the carbon-coated TiO_2, as compared with P25. For TC-900, the absorption is weak in the visible region, which might be a result of the lower carbon content. With the increase in the carbon content in the TC samples, the absorption intensity becomes more pronounced, while the absorption edge, due to the anatase TiO_2, becomes less predominant. All the composites show clearly the UV absorption band of anatase.

Raman spectroscopy is a powerful technique for the investigation of various phases of TiO_2. From a measurement of the maximum of the low-frequency Raman band it is

(15) Inagaki, M.; Hirose, Y.; Matsunaga, T.; Tsumura, T.; Toyoda, M. *Carbon* **2003**, *41*, 2619.
(16) Tsumura, T.; Kojitani, N.; Izumu, I.; Iwashita, N.; Toyoda, M.; Inagaki, M. *J. Mater. Chem.* **2002**, *12*, 1391.
(17) Lin, J.; Lin, Y.; Liu, P.; Meziani, M. J.; Allard, L. F.; Sun, Y. *J. Am. Chem. Soc.* **2002**, *124*, 11514.

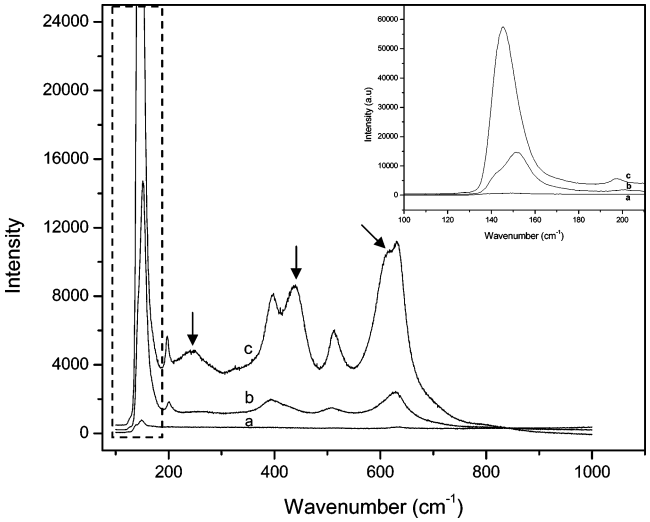

Figure 3. Raman spectra of TiO_2@C composite prepared at (a) 700, (b) 800, and (c) 900 °C. Inset shows an expanded part marked with dotted lines of low-frequency mode of TiO_2. Arrows show the coexistence of rutile phase.

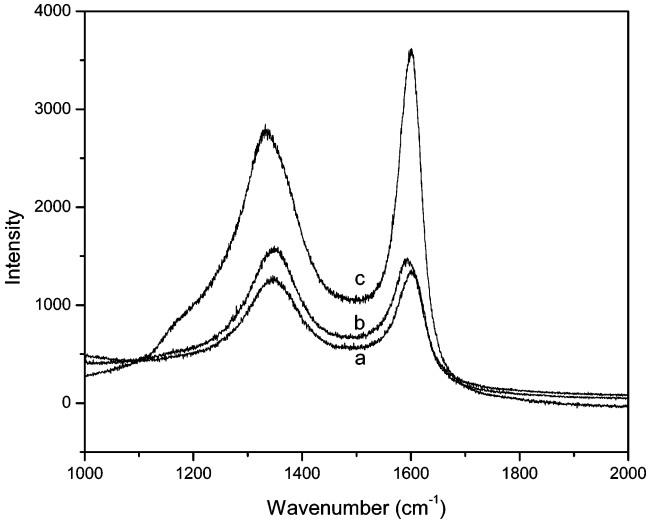

Figure 4. Raman spectra showing graphitic modes in TiO_2@C composite prepared at (a) 700, (b) 800, and (c) 900 °C.

possible to determine the nanoparticles size.[18] It is known that the particle size can cause large shifts in the location of the scattered Raman peaks and their widths.[19,20] According to the symmetry group analysis, anatase TiO_2 has 15 optical modes in Raman (the irreducible representation $1A_{1g} + 1A_{2u} + 2B_{1g} + 1B_{2u} + 3E_g + 2E_u$). The modes A_{1g} (519 cm^{-1}), B_{1g} (399 and 519 cm^{-1}), and E_g (144, 197, and 639 cm^{-1}) are Raman-active and thus six fundamental transitions are expected in the Raman spectrum of anatase.[21] The four modes A_{1g} (612 cm^{-1}), B_{1g} (143 cm^{-1}), B_{2g} (826 cm^{-1}), and E_g (447 cm^{-1}) are Raman-active modes of rutile.[22] Figure 3 shows the Raman spectra of the composite samples prepared at different temperatures, the observed peaks are similar to those of bulk anatase with red shift. As the temperature increases, the intensity of the lowest frequency peak, 148 cm^{-1}, dramatically increases, indicating the enhancement of crystallinity. As shown in Figure 3, TC-700 exhibits three Raman bands at 148.6 (E_g), 513.8 (E_g), and 631.7 (E_g) cm^{-1}, which correspond to the typical Raman fingerprint of anatase at room temperature. The sample prepared at 800 °C reveals more intense peaks at 148, 200, 264, 393, 507.8, and 629.7 cm^{-1}. The TC-900 product shows characteristic anatase peaks. It also illustrates peaks at 246 and 437 cm^{-1} and a shoulder at 616.5 cm^{-1} (the peaks are marked by arrows in Figure 3), which correspond to the E_g and A_{1g} modes of the rutile phase, respectively. These observations suggest that the phase transformation from anatase to rutile occurs in TiO_2@C samples at 900 °C. It is reported that the transition temperature from anatase to rutile for TiO_2 will occur for annealing temperatures above 600 °C.[15] The presence of carbon inhibits the formation of the rutile phase which starts to form only at 900 °C. The reason that the rutile phase was not detected in the XRD analysis of TC-900 is perhaps due to the fact that its concentration is less than 5%, which is the XRD detection limit. Another explanation for XRD not being able to find the rutile phase is because XRD usually reveals the long-range order of materials and gives average structural information. Raman spectroscopy can be a local probe, and it is very sensitive to crystallinity and microstructures of materials.

In the case of anatase TiO_2 nanoparticles the low-frequency peak 144 cm^{-1} shows a strong dependence on the quantum size confinement effects.[23] Several groups have applied phonon confinement model and stoichiometry of TiO_2 for the correlation between the shift and width of the E_g anatase mode at 144 cm^{-1} and the crystalline domain size.[24,25] It is clear from the inset of Figure 3 that this low-frequency peak blue shifts and the line width increases as the temperature is raised. This observation suggests that the particle size is decreasing. A similar behavior of frequency shift was observed for TiO_2 nanoparticles prepared by sol−gel techniques.[24] The width of TC samples was calculated and presented in Table 1. It also concurs with the decrease in particle size evidenced from the blue shift.

The presence and nature of carbon in the TiO_2@C sample were also investigated by Raman spectroscopy. The carbon exhibits characteristic Raman peaks at around 1346 and 1593 cm^{-1} which originate from the disordered and ordered graphitic carbon, respectively. The peak at around 1593 cm^{-1} corresponds to an E_{2g} mode of graphite, which is due to the sp^2-bonded carbon atoms in a two-dimensional hexagonal graphitic layer.[26] The D band at around 1346 cm^{-1} is

(18) Turkovic, A.; Ivanda, M.; Popovic, S.; Jonejc, A.; Gotic, M.; Dubcek, P.; Music, S. *J. Mol. Struct.* **1997**, *410*−*411*, 271. Gotic, M.; Ivanda, M.; Popovic, S.; Music, S.; Sekulic, A.; Turkovic, A.; Furic, K. *J. Raman Spectrosc.* **1997**, *28*, 555. Music, S.; Gotic, M.; Ivanda, M.; Popovic, S.; Turkovic, A.; Trojko, R.; Sekulic, A.; Furic, K. *Mater. Sci. Eng. B* **1997**, *47*, 33.
(19) Iida, Y.; Furukawa, M.; Aoki, T.; Sakai, T. *Appl. Spectrosc.* **1998**, *52*, 673.
(20) Bersani, D.; Lottici, P. P.; Ding, X.-Z. *Appl. Phys. Lett.* **1998**, *72*, 73. Balachandran, U.; Eror, N. G. *J. Solid State Chem.* **1986**, *42*, 276.
(21) Oksaka, T.; Izumi, F.; Fujiki, Y. *J. Raman Spectrosc.* **1978**, *7*, 321. Berger, H.; Tang, H.; Kevy, F. *J. Cryst. Growth* **1993,** *130*, 108.
(22) Porto, S. P. S.; Fbeury, P. A.; Damen, T. C. *Phys. Rev.* **1967**, *154*, 522. Hara, Y.; Nicol, M. *Phys. Status Solidi B* **1974**, *94*, 317.
(23) Bassi, A. L.; Cattaneo, D.; Russo, V.; Bottani, C. E.; Bartoriri, E.; Mazza, T.; Pisen, P.; Midani, P.; Ernst, F. O.; Wegner, K.; Pratsinis, S. E. *J. Appl. Phys.* **2005**, *98*, 74305.
(24) Zhang, W. F.; He, Y. L.; Zhang, M. S.; Chen, Q. *J. Phys. D: Appl. Phys.* **2000**, *33*, 912.
(25) Parker, J. C.; Sieger, R. W. *Appl. Phys. Lett.* **1990**, *57*, 943. Parker, J. C.; Sieger, R. W. *J. Mater. Res.* **1990**, *5*, 1246.

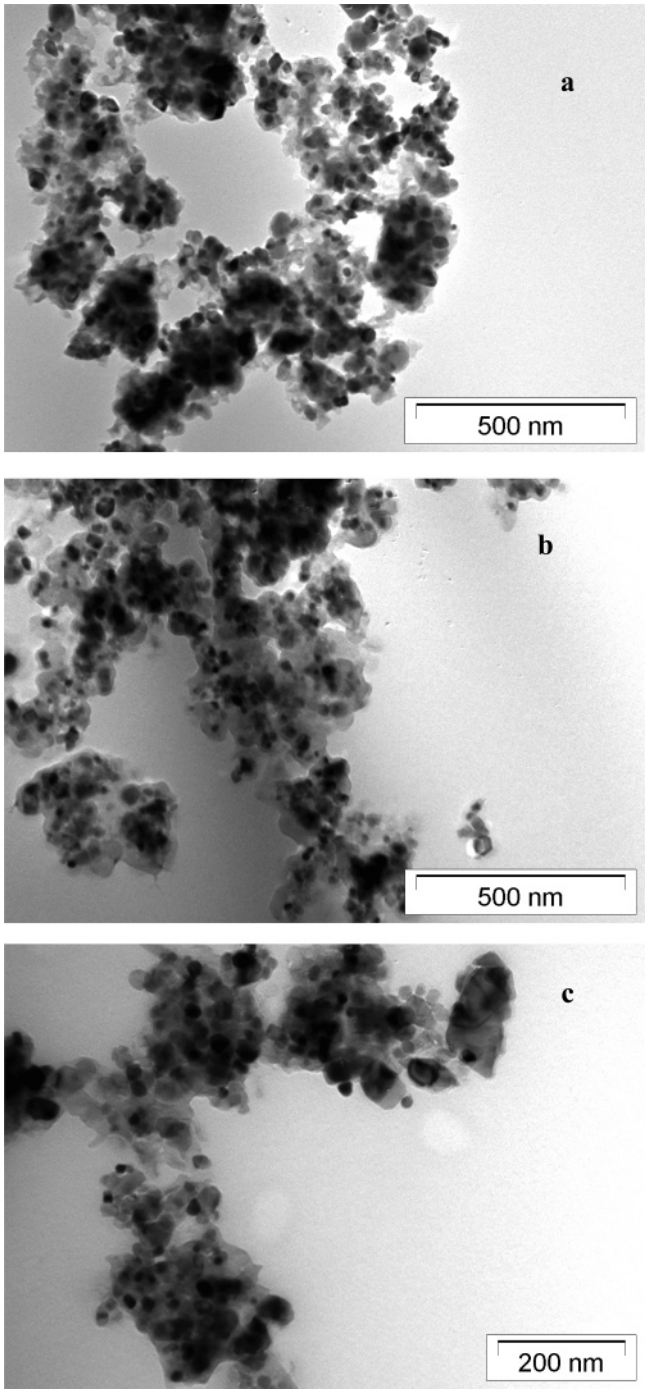

Figure 5. TEM images of TiO_2@C composites prepared at (a) 700, (b) 800, and (c) 900 °C.

associated with the presence of defects in the hexagonal graphitic layers. It is clear from Figure 4 that as the temperature increases, more intense peaks are observed. The graphitic peak becomes more intense than the disordered carbon peak as the temperature is raised.

Figure 5 shows the TEM images of TiO_2@C composite prepared at different temperatures. It can be seen from the micrographs that the dark shapes, TiO_2, are surrounded by carbon layers. The diameter of these TiO_2 nanoparticles is in the range of 15−35 nm surrounded by an ∼2 nm carbon layer. In general, the particle size increases as the reaction temperature increases. However, in the present study we observed that the particle size decreases as the temperature increases from 700 to 800 and to 900 °C. At high temperatures, the rate of formation of TiO_2 is faster, giving rise to smaller particles. As soon as the TiO_2 crystallizes, the free carbon present in the reaction mixture will condense over the TiO_2 surface, thus avoiding the particle agglomeration. HRTEM results are presented in Figure 6, indicating that a few of the graphitic layers surround the anatase TiO_2. The *d* spacing of graphitic layers is 0.341 nm, which is in agreement with that reported the literature. The measured distance between TiO_2 (101) lattice planes is 0.352 nm, which is very close to the distance value of 0.351 nm reported for anatase TiO_2 (JCPDS file No. 89-4921). It is clear from the HRTEM measurements that crystallinity increases as the temperature increases, which is in good agreement with our XRD results. The respective selected area electron diffraction patterns are presented in Figure 6. We observed a ring pattern along with a spot pattern for all three samples, indicating the polycrystalline nature of the nanoparticles.

Figure 7a depicts the N_2 adsorption−desorption isotherms with a hysteresis loop, indicating the mesoporous nature of composite TC samples. It is also evident that a considerable hysteresis loop at a high relative pressure confirms the existence of the macroporous (>50 nm, according to IUPAC) nature of prepared samples. The mesopores and nanoparticles coexist in the TC composite samples. The hysteresis loops can be attributed to the total contribution of both interparticle and intraparticle pores. As can be seen from Figure 7a, the hysteresis loop occurs at higher P/P_0 values for TC-900 than for TC-800 and TC-700. The BET surface area, pore size, and pore volume are given in Table 1. There is no appreciable change in the surface area of TiO_2@C as a function of the reaction temperature; however, the pore volume is largely dependent on the temperature. As the temperature increases from 700 to 900 °C, the pore volume increases.

The pore size distribution was measured by BJH desorption isotherms. The pore size distributions of TC samples prepared at different temperatures is presented in Figure 7b. The sample prepared at 700 °C has unimodal, narrow pore size distribution with a maximum around 15 nm, whereas in samples prepared at 800 and 900 °C the pore size distribution is also unimodal but with a broader pore size distribution with a maximum at around 29 and 39 nm, respectively. As the temperature increases, the pore size distribution is changed from 15 to 39 nm.

The formation of TiO_2@C core−shell-like structures by the present method can be explained based on TEM, HRTEM, and Raman spectroscopy analysis. It is clear that the TC product, after the thermal dissociation of Ti(IV) oxyacetyl acetonate, is composed of a TiO_2 core surrounded by a few graphitic carbons. The thermal decomposition of Ti oxy acetyl acetonate takes place at a temperature above 500 °C, forming a vapor of Ti, oxygen, and carbon. The next stage is the formation of metallic Ti particles by vapor nucleation and condensation, and particle coagulation processes. In the high-temperature zone, the process of the dissolution of the released oxygen in the Ti particles occurs,

(26) Reznik, D.; Olk, C. H.; Neumann, D. A.; Copley, J. R. D. *Phys. Rev. B* **1995**, *52*, 116.

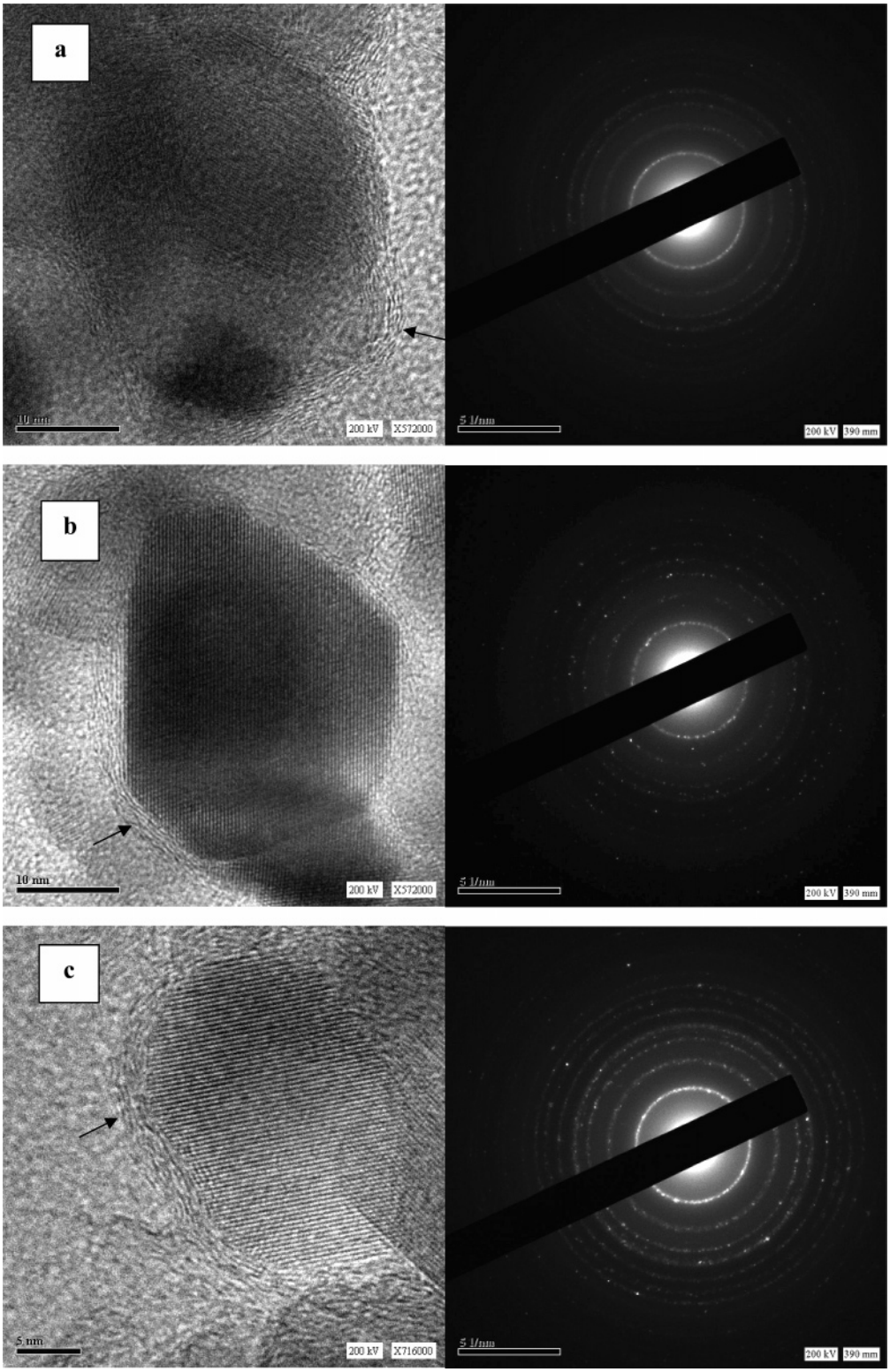

Figure 6. HRTEM images of TiO_2@C composites prepared at (a) 700, (b) 800, and (c) 900 °C. Arrows show the graphitic layers on the TiO_2. Respective electron diffraction patterns are shown.

yielding TiO_2. The final product of the reaction is determined during the cooling and is related to carbon segregation in the supersaturated particles due to the reduction in solubility as the system's temperature decreases. The dissolved carbon contributes to the flux of carbon atoms toward the particle surface upon cooling. Additionally, there is another flux, the surface flux, which is limited by the diffusion of carbon atoms on the surface, seeking their lowest energy states.[27] If the cooling rate is infinitely slow, then the achieved particle structure after carbon segregation would be graphitic carbon around a TiO_2 particle, that is, the equilibrium structure. However, due to competition between the segregation and surface fluxes, two situations can occur in the system upon

(27) Gavillet, J.; Loiseau, A.; Ducastelle, F.; Thair, S.; Bernier, P.; Stephan, O. *Carbon* **2002**, *40*, 1649.

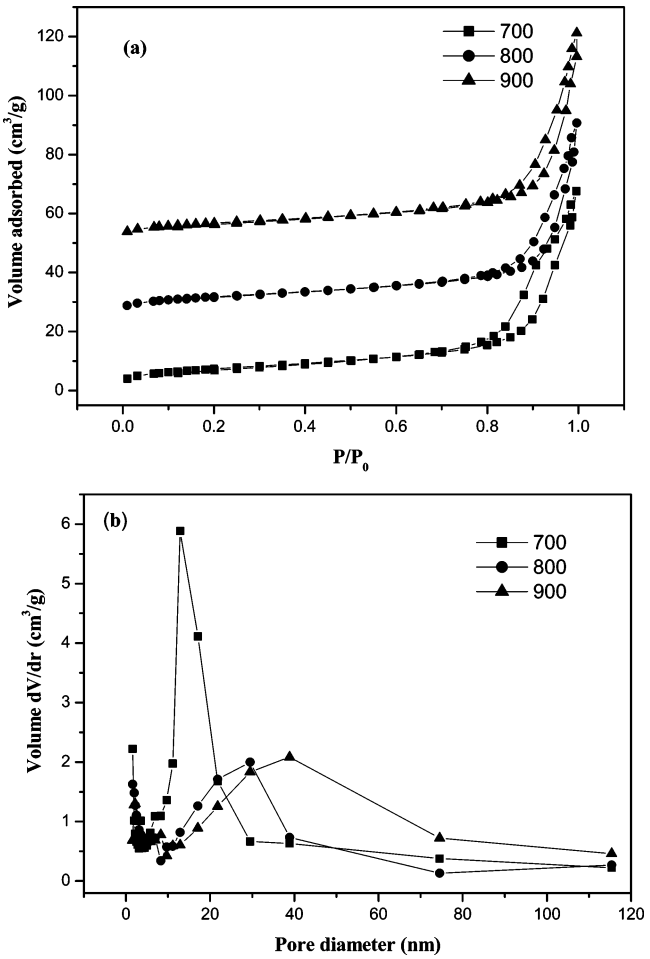

Figure 7. (a) Nitrogen adsorption−desorption isotherms and (b) Barret−Joyner−Halenda (BJH) pore size distribution plots of TiO_2@C composites prepared at different temperatures.

cooling. It can form carbon core and TiO_2 shell or TiO_2 core with carbon shell; it is known that the crystallization of TiO_2 is faster than the carbon; thus, first TiO_2 crystallizes and next carbon is crystallizing, giving rise TiO_2@C core−shell-like structures.

Chlorophenols (CPs) are common organic contaminants, which show low biodegradability, and therefore are persistent pollutants, posing serious risks to the environment once mixed into natural water.[28] These compounds are carcinogenic and mutagenic and have a tendency to accumulate in fatty tissue.[29] Many efforts have been dedicated to the study of alternative technologies that are able to minimize the deleterious effect caused by this anthropic material. Using the conventional technique to eliminate these kinds of compounds may be difficult as they are usually present at low concentrations in water, or they are especially refractory to the oxidants. Monochlorophenols are mainly used as intermediates in dyestuffs and in the manufacture of higher chlorinated phenols such as 2,4-dichlorophenol (DCP), which is used in larger volumes in the manufacturing of 2,4-dichlorophenoxyacetic acid.[30] Therefore, it has been necessary to develop more effective processes for the destruction of such contaminants.

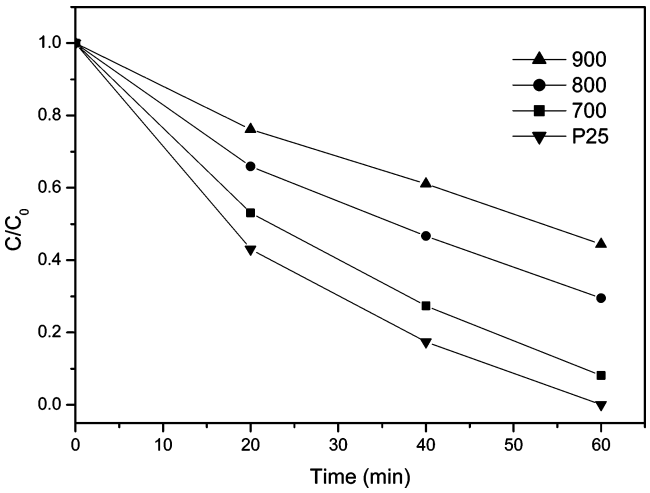

Figure 8. Photocatalytic degradation of 4-chlorophenol on TiO_2@C composites prepared at different temperatures as well as the P25 TiO_2 for comparison.

The photocatalytic activities of a TiO_2@C composite were evaluated by the degradation of 4-cholorphenol in aqueous solution. The photocatalytic decomposition of 4-chlorophenol was followed by HPLC. For comparison, the photocatalytic activity of commercial P25 was also measured under identical conditions. The catalytic activities of TiO_2@C and P25 are presented in Figure 8. The photocatalytic activity of TiO_2@C prepared at 700 °C was comparable to that of P25; other composites showed lower activity than that of P25. The comparable activity of TC-700 can be explained on the basis of surface area and pore size. The photocatalytic activity can be dependent on various factors such as surface area, phase structure, and crystalline size and pore size.[31] The composite prepared at 700 °C had high activity among prepared composites and can be attributed to the high carbon content and high surface area of TC-700. For effective degradation, the organic material should be preconcentrated on the surface of the semiconductor particle to effectively utilize the excitons which are generated on the surface of the semiconductor. The high carbon content on the surface of TC-700 could accommodate large amounts of 4-chlorophenol, exhibiting high activity compared with other TiO_2@C.

Methylene blue (MB) photodecomposition was also carried out with the TC samples under sunlight and the results are shown in Figure 9. During 1 h, the photobleaching of the solution was followed by UV−visible spectroscopy. It is worth noting that the photobleaching of methylene solution is completely over within 1 h on the TC-900. The methylene blue concentration decrease is larger for the TC-900 sample than other TC samples. Photodecomposition of all TC samples showed higher activity than Degussa P25. We have derived the apparent reaction rate constants for the photobleaching of MB from the linear slope of the relationship between $\ln(c/c_0)$ and kt, where c_0 and c are the concentrations

(28) Hugul, M.; Boz, I.; Apak, R. *J. Hazard. Mater. B* **1999**, *64*, 313. Benitez, F. J.; Beltran-Heredia, J.; Acero, J. L.; Javier Rubio, F. *Chemosphere* **2000**, *41*, 1271.
(29) Vernard, T. R., Jr.; Schreiner, A. F.; Xie, T. Y.; Chen, C. L.; Gratzl, J. S. *J. Photochem. Photobiol. A: Chem.* **1995**, *90*, 183.
(30) Pandian, T.; Rivas, O. M.; Martines, J. O.; Amezuca, G. B.; Matrinez-Carrillo, M. A. *J. Photochem. Photobiol. A: Chem.* **2002**, *146*, 149.
(31) Yu, J. C.; Yu, J. G.; Ho, W. K.; Zhang, L. Z. *Chem. Commun*. **2001**, 1942. Yu, J. C.; Yu, J. G.; Ho, W. K.; Zhang, L. Z. *J. Photochem. Photobiol. A* **2002**, *148*, 263.

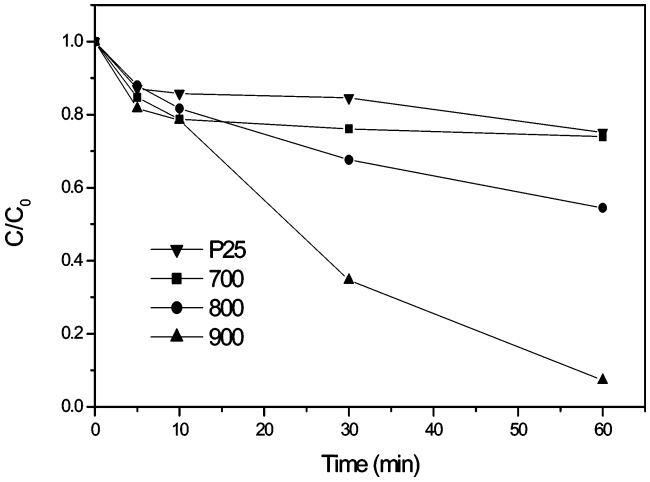

Figure 9. Photochemical activities of various TiO_2@C compoistes for MB bleaching under sunlight irradiation.

of initial solution and after *t* (min) of irradiation, respectively. The values of the rate constants of the MB degradation are given in Table 1. All the TC samples exhibited higher *k* value than the P25. The difference in the activity can be explained by the textural properties of the TC-900 sample. As Table 1 shows, the particle sizes and pore volumes are higher than the other TC samples. It is known from the literature that the crystalline nature also plays an important role in the photocatalytic activity of TiO_2. As the synthesis temperature increases, the absorption in visible region is predominant in TC samples compared to that of P25; thus, higher photocatalytic activity is observed. P25 cannot absorb the visible light; thus, it showed low activity for the MB photodecomposition. On the other hand, the TC samples showed higher activity. Among the TC samples, TC-900 showed higher reaction rate; this may be attributed to the smaller particle size, better crystallinity, and low carbon content. The TC-900 has broad pore size distribution, with a maximum of 39 nm. The more methylene blue can easily diffuse into large pores and reach the active sites effectively, on other hand, TC-700 exhibits lower activity; this could be attributed to the low crystallinity, larger particle size, and smaller pore size. The lower carbon content is manifested in a thinner coating layer, enabling the solution to get to the active site easier and faster. The presence of carbon on TiO_2 is found to have an influence on the activity of the titania in the visible region only, whereas in the 4-chlorophenol decomposition of TC composites it exhibits lower activity than P25. The carbon shell on TiO_2 shows a certain advantage, namely, the phase suppression, enhancing the adsorption of pollutants and also manifesting the fate of surface charge carriers on TiO_2 nanoparticles.

Conclusions

TiO_2@C core−shell-like structures were prepared in a single-step pyrolysis of titanium(IV) oxyacetyl acetonate in a Swagelok cell at various temperatures. XRD measurements show that all TC samples exhibit anatase TiO_2. Raman analysis reveals that the sample prepared at 900 °C contains a mixture of anatase and rutile phase. The stabilization of anatase is due to the carbon layers wrapped around the TiO_2. As the temperature increases, the surface area and carbon content decrease. The sizes of the composite samples are in the range of 15−35 nm. The sample prepared at 700 °C exhibits a narrow pore size distribution, while the samples obtained at 800 and 900 °C showed a broad pore size distribution. The photochemical activities of TC samples have been evaluated by photochemical decomposition of 4-chlorophenol and methylene blue. The TC-700 had comparable activity with P25 for the 4-chlorophenol decomposition; however, all the TC samples exhibited higher activities than P25 for methylene blue photobleaching studies. Among the TC samples, TC-900 exhibited higher photochemical activity because of a better crystalline nature and lower carbon content.

Acknowledgment. The authors thank Dr. Yudith Grinblat and Dr. Tova Tamari for the HRTEM and TEM analysis. S.S. is thankful to the Research Authority, Bar-Ilan University, for the Samuel and Helene Soref Young Scientist fellowship.

CM052790N